A Low-Complexity PFA-Based Autofocus Algorithm for Automotive SAR

S. Hamed Javadi, *Member, IEEE*, André Bourdoux, *Senior Member, IEEE*, Adnan Albaba, and Hichem Sahli

***Abstract*—Radars provide robust perception of vehicle surroundings by effectively functioning in poor light and adverse weather conditions. Synthetic aperture radar (SAR) algorithms are used to address the limited angular resolution of radars by enlarging antenna aperture size synthetically as the radar moves. An autofocus algorithm is essential to improve the SAR image quality by compensating for errors mainly caused by inaccurate radar localization. Existing autofocus algorithms are mostly tailored for the frequency-domain SAR techniques which are prevalent in aviation and spaceborne applications, thanks to their lower complexity in large data processing. However, in the automotive context, the backprojection algorithm (BPA) is often preferred since it provides less distorted images at the cost of more complexity. Addressing the gap in efficient autofocus solutions for time-domain algorithms, this article introduces a dual-layered autofocus strategy that integrates the polar format algorithm (PFA) with BPA. The first layer uses a novel localization error compensation autofocus (LECA) processing pipeline to estimate and correct the localization errors within the PFA domain, leveraging its computational efficiency. The second layer seamlessly transfers these corrections to BPA, enabling high-quality SAR imaging while maintaining low complexity. In addition, the strategy extends phase gradient autofocus (PGA) techniques to enhance the efficiency of localization error compensation for BPA. Validated through real-world automotive experiments, the proposed pipeline delivers state-of-the-art image focus and resolution, setting a new benchmark for computationally efficient SAR imaging.**

***Index Terms*—Autofocus, backprojection algorithm (BPA), frequency-modulated continuous wave (FMCW), multiple-input-multiple-output (MIMO), phase gradient autofocus (PGA), polar format algorithm (PFA), radar imaging, synthetic aperture radar (SAR).**

I. Introduction

A. Motivation

RADARS operate independently of lighting conditions and can penetrate fog. They achieve cm-level range resolution using the wide bandwidth available at mm-wave frequencies. These benefits come at a low cost, making radar an essential modality in complex multisensor systems, such as in automotive applications [1] where robust and reliable environmental perception is critical. Specifically, the advent of advanced driver assistance systems (ADAS) in autonomous driving has significantly increased interest in frequency-modulated continuous-wave (FMCW) radars due to their simple receiver design and the reduced data rate requirements for analog-to-digital converters (ADCs) [2].

While range resolution depends solely on bandwidth, achieving fine angular resolution requires a large radar aperture. This large aperture is impractical at low frequencies and expensive at mm-wave frequencies due to front-end complexities. An alternative solution is a synthetic aperture radar (SAR) algorithm, which effectively enlarges the aperture using the radar motion [3]. In SAR, radar data are collected over time from different locations as the radar moves, synthesizing a larger aperture size.

The first practical SAR implementation probably dates back to 1978 when it was used in spaceborne applications for oceanographic purposes [4]. Since then, different SAR algorithms, ranging from Doppler beam sharpening (DBS) to matched filter (MF) [5], have emerged each offering different compromises between image quality and complexity. Nevertheless, they are all plagued by phase errors mainly[1] due to positioning errors, leading to defocused images.

While MF requires a fourfold integration over an area of interest (AoI), the backprojection algorithm (BPA) [6] provides a less-complex alternative by backprojecting the range-compressed data into the image pixels and accumulating them after Doppler compensation. Despite its relatively high complexity, BPA is widely used, thanks to its ability to produce high-resolution images. At the lower end of the complexity spectrum is DBS, which simply applies a 2-D Fourier transform (FT) to the radar data, though it is limited to small angular coverage. In contrast, the polar format algorithm (PFA) [7] enhances the SAR image quality by correcting the distortions in DBS caused by wavenumber dependencies.

In this article, we use the PFA as an efficient SAR solution for automotive applications. We address autofocus challenges by proposing two optimized techniques to enhance PFA autofocus performance. Finally, we integrate the refined PFA autofocus results into the BPA to generate high-resolution images.

B. Related Works

Recent advancements in automotive SAR systems have focused on improving resolution, reducing hardware size, and

Received 19 February 2025; revised 15 April 2025; accepted 23 May 2025. Date of publication 30 May 2025; date of current version 10 June 2025. This work was supported by the Horizon Europe Project *Edge AI Technologies for Optimised Performance Embedded Processing* under Grant 101097300. *(Corresponding author: S. Hamed Javadi.)*

S. Hamed Javadi, AndréBourdoux, and Adnan Albaba are with the Interuniversity Micro-Electronics Center (IMEC), 3001 Leuven, Belgium (e-mail: hamed.javadi@imec.be; andre.bourdoux@imec.be; adnan.albaba@imec.be).

Hichem Sahli is with the Interuniversity Micro-Electronics Center (IMEC), 3001 Leuven, Belgium, and also with the Department of Informatics, Vrije Universiteit Brussel (VUB), 1050 Brussels, Belgium (e-mail: hichem.sahli@imec.be).

Digital Object Identifier 10.1109/TRS.2025.3574010

[1] In the mm-wave frequencies.

integrating SAR with other sensor technologies such as LiDAR and optical cameras [8]. In addition, SAR can operate under conditions where optical and LiDAR systems may struggle, such as in low visibility or adverse weather conditions. This makes SAR a critical component in the sensor fusion strategies used in modern autonomous driving systems [9].

An automotive SAR has been used in [10] for parking application where the vehicle trajectory is estimated by a secondary radar in the front bumper of the vehicle while the side radar runs BPA. Using a multiple-input-multiple-output (MIMO) FMCW radar, it is proposed by [11] to detect AoI first by conventional MIMO processing and then use BPA for automotive SAR. Tebaldini et al. [9] compare three algorithms for combining low-resolution images from an MIMO radar to form a single SAR image. These algorithms include the fast factorized backprojection (FFBP), the 3D2D scheme, and the quick and dirty (Q&D) method. The study provides a detailed mathematical description of each algorithm along with their evaluations based on open road campaign data. However, a more comprehensive automotive MIMO-SAR has been outlined by Zhang et al. [12] where the pixelwise phase difference among different channels is compensated to increase the signal-to-noise ratio (SNR) by coherent processing before backprojection.

Polisano et al. [13], [14] propose to achieve an extremely fine resolution by mitigating grating lobes due to radar silence in a large SAR coherent processing interval (CPI) by spectrum approximation using compressive sensing. Tagliaferri et al. [15] present a multisensor fusion technique that combines data from global navigation satellite system (GNSS), inertial measurement units (IMUs), odometers, and steering angle sensors to improve positioning accuracy. The experimental results demonstrate that this approach achieves cm-level accuracy in urban environments.

The methods discussed rely on a highly precise navigation system for SAR. While current automotive technology provides centimeter-level accuracy, which may be sufficient for short-range SAR imaging, the navigation rate is significantly lower than the radar pulse repetition frequency (PRF). In addition, navigation signals may be unavailable in certain areas, and this level of accuracy is insufficient for long-range SAR imaging [16]. Therefore, the use of an autofocus algorithm is essential to improve the SAR image quality [17].

On the other hand, SAR algorithms have evolved, thanks to their diverse aviation and space applications where the frequency-domain techniques have been prevalent due to their lower complexity in handling large data [18]. Consequently, autofocus methods have mostly been developed for frequency-domain techniques [13], [19], [20], [21], [22], [23], while fewer exist for time-domain techniques. Notably, time-domain BPA is often preferred for automotive applications, with specific examples provided later to illustrate the reasons for this preference. A potential solution for BPA autofocus could involve using matched-filtering across the radar locations within the CPI. However, the complexity of this method might be greater than that of BPA, rendering it impractical. In this article, we propose using the phase gradient autofocus (PGA) [19], [20] on top of PFA and using the phase error correction for BPA. This approach offers a computationally efficient autofocus algorithm suitable for BPA.

PGA [19], [20] is widely used because it is fast. It assumes that each range bin is dominated by at most one major scatterer and proves that the phase error spectrum is modulated by that major scatterer. Then, it uses the redundancy across the image major scatterers to estimate the phase error gradient based on which the phase error is estimated.

While computationally efficient, PGA may fail in cases with low SNRs. In these cases, parametric solutions may perform better at a cost of more complexity. The minimum entropy autofocus (MEA) [22] assumes that the phase error is quadratic and estimates the quadratic phase error by minimizing the image entropy (IE). Instead of the IE, other image sharpness metrics can be used for the image quality enhancement [23].

C. Summary of Contributions and Article Organization

The contributions of this article are summarized as follows.

1) We introduce a signal model for localization errors in PFA, demonstrating that these errors manifest in the cross-range dimension.
2) Building on this model, we propose the localization error compensation autofocus (LECA) algorithm for PFA, which optimizes image contrast (IC)—as image quality metric—to estimate localization errors. We show that compensating for velocity-related errors is particularly crucial.
3) We propose using the localization errors calculated by LECA in BPA. Since PFA is less complex than BPA, the use of PFA significantly reduces the complexity of BPA autofocus.
4) Given the efficiency of PGA, we propose to estimate the phase error by PGA and use it for the compensation of the localization errors of BPA. This makes the BPA autofocus further efficient.
5) The effectiveness of the proposed autofocus algorithms is validated through evaluations in an automotive scenario in various SAR processing pipelines.

While the individual components of the proposed method—PFA, BPA, and PGA—are widely recognized and mature techniques in SAR imaging, their strategic integration within a dual-layered autofocus pipeline presents a novel approach to optimizing automotive SAR imaging. This integration allows for an efficient correction of localization errors, ensuring improved resolution without incurring excessive computational costs.

The remainder of this article is organized as follows. Section II presents the fundamentals of FMCW radars and radar imaging with them. Our proposed autofocus algorithms are elaborated in Section III with their evaluation results presented in Section IV. Finally, this article is concluded in Section V with future directions toward further improvements.

II. Background

A. FMCW Radars

In FMCW radars, N_c chirps are transmitted during each CPI. Each chirp is a continuous wave with frequency starting from

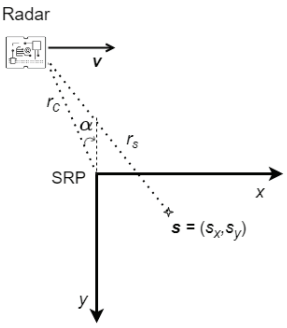

Fig. 1. SAR 2-D geometry. SRP indicates the SAR origin and stands for the SAR reference point.

f_c and linearly increasing to $f_c + B$ with B being the radar bandwidth. Accordingly, the transmitted chirp is modeled by

$$s_T(t) = a_c \exp\left[j\left(\omega_c + \frac{\gamma}{2}t\right)t\right] \tag{1}$$

where a_c denotes the chirp amplitude, $\omega_c \triangleq 2\pi f_c$ is its starting angular frequency, and γ is its slope.

The received echo signal from a specific scatterer $\boldsymbol{s}$ with round-trip time τ_s is given by

$$s_R(t) = \sigma(\boldsymbol{s}) \exp\left[j\left(\omega_c + \frac{\gamma}{2}(t-\tau_s)\right)(t-\tau_s)\right] \tag{2}$$

wherein the scatterer's reflectivity, the system gains, and the propagation effects are included in $\sigma(\boldsymbol{s})$ for convenience. The received signal is demodulated to give the beat signal as follows:

$$\begin{aligned} s_B(t) &= s_T^*(t)\, s_R(t) \\ &= \sigma(\boldsymbol{s}) \exp\left[-j\tau_s\left(\omega_c + \gamma t - \frac{\gamma}{2}\tau_s\right)\right] \end{aligned} \tag{3}$$

where $s_T^*(t)$ is the complex conjugate of $s_T(t)$. The maximum unambiguous range of an FMCW radar is given by $r_{\max} = (\pi c F_s/\gamma)$ with F_s and c being the sampling rate and the light speed, respectively. This gives $(\gamma/2)\tau_s = (\pi c F_s/r_{\max}) \times (2r_s(t)/c) = (r_s(t)/r_{\max})2\pi F_s$ where $r_s(t)$ is the slant range to the scatterer $\boldsymbol{s}$. This implies that the term $\gamma\tau_s/2$ is negligible compared with ω_c, especially since F_s is in the range of at most several MHz.[2]

Therefore, the beat signal can be approximated by

$$s_B(i,n) \approx \sigma(\boldsymbol{s}) \exp\left[-j\frac{2}{c}(\omega_c + \gamma T_s i)\, r_s(n)\right] \tag{4}$$

where T_s denotes the receiver sampling period and the model has been discretized in fast time index i and slow time index (viz. chirp number) n.

B. SAR Imaging With FMCW Radar

As mentioned above, diverse SAR algorithms, ranging from DBS to MF, offer various tradeoffs between image quality and computational complexity. While DBS is too limiting regarding angular coverage and MF is computationally intensive, the PFA strikes a balance by enhancing image quality through wavenumber distortion corrections while maintaining manageable complexity.

1) PFA: The PFA leverages the geometric properties of SAR imaging to correct wavenumber distortions and improve image quality. As illustrated in the 2-D geometry in Fig. 1, the slant range to a scatterer, $r_s(n)$ in (4), can be approximated by projecting the scatterer's position onto the radar line of sight (RLOS). This projection is expressed as $r_s(n) = r_c(n) + y_s\cos(\alpha) + x_s\sin(\alpha)$ with $r_c(n)$ and α being the radar range to the SAR reference point (SRP) and its squint angle, respectively. Then, compensating the beat signal with respect to $r_c(n)$ gives

$$\begin{aligned} &s_C(i,n) \\ &\quad\triangleq s_B(i,n)\exp\left[\mathrm{j}\mathrm{k}(i)\, r_c(n)\right] \\ &\quad= \int_{x_s}\int_{y_s} \sigma(x_s,y_s)\exp\left[-j\left(k_x(i,n)\,x_s + k_y(i,n)\,y_s\right)\right]\mathrm{d}x_s\mathrm{d}y_s \end{aligned} \tag{5}$$

wherein the integration is taken over all the scatterers in the radar's FoV. In (5), $k(i) \triangleq (2/c)(\omega_c + \gamma T_s i)$ is the wavenumber (i.e., the spatial phase rate [7]) with its components $k_x(i,n) \triangleq k(i)\sin(\alpha_n)$ and $k_y(i,n) \triangleq k(i)\cos(\alpha_n)$, respectively, and n represents the chirp index, and the dependency of the squint angle α on the chirp number n has been emphasized.

The signal model (5) has the form of a 2-D FT but with co-dependent spatial frequencies (i.e., the wavenumbers). Specifically, $k_x(i,n)$ and $k_y(i,n)$ form a polar format, where the amplitude is given by $k(i)$, and the phase varies with n. To enable fast FT (FFT), the indices i and n are redefined into i' and n', respectively. This allows the range-compensated signal, $s_C(i,n)$, to be interpolated onto a grid of wavenumbers, $k_x[n']$ and $k_y[i']$.[3] Consequently, an image of the target scene is reconstructed by performing a 2-D inverse FFT (IFT) from the interpolated signal $s_C[i',n']$

$$\sigma(x_s,y_s) = \text{2D-IFT}\left\{s_C\left(i',n'\right)\right\}. \tag{6}$$

The extension of the 2-D configuration shown in Fig. 1 to 3-D can be achieved by scaling the wavenumbers with $\cos(\psi_n)$, where ψ_n represents the radar grazing angle for each chirp.

2) BPA: The BPA is a time-domain SAR imaging method known for its ability to produce high-resolution images. BPA begins by defining an image grid representing the target scene. For each chirp and image pixel, the range profile is interpolated based on the radar's data. The image pixel is then reconstructed by summing the interpolated range profiles across all the chirps, with appropriate compensation for the phase term. Mathematically, the range profile of the beat signal (4) is given by its FT along the fast time index

$$G(v,n) = \mathrm{FT}\{s_B(i,n)\} \tag{7}$$

with v denoting the range index. Then, the image pixel in the grid location (x_p,y_p) is reconstructed by

$$\sigma\left(x_p,y_p\right) = \sum_n G\left(v',n\right)\exp\left(j\frac{2\omega_c r_{p,n}}{c}\right) \tag{8}$$

wherein v' indicates a fractional index used for interpolating the range profile $G(v,n)$ at the pixel location and $r_{p,n}$ is the

[2]This term results in the residual video phase error (RVPE). Here, we reason that this error is negligible in the current technology of mm-wave FMCW radars.

[3]Further details can be found in [7].

range to the pixel at the instance of the n'th chirp. Equation (8) must be applied for all the pixels of the image grid.

III. Localization Error Compensation Autofocus

In this section, we first discuss the problem statement, and then propose the LECA for PFA. Finally, we extend the idea to BPA.

A. Problem Statement

We highlight that positioning errors in automotive SAR systems are inevitable due to insufficient accuracy and data rate of the automotive navigation systems. This necessitates the application of an appropriate autofocus algorithm to compensate for those errors. However, the state-of-the-art efficient autofocus algorithms are tailored for the frequency-domain SAR techniques.

Accordingly, the problem considered here is 1) the derivation of a model explicitly showing the impact of the localization error on the SAR imaging quality and 2) devising an effective and meanwhile computationally simple autofocus framework for the automotive SAR. We remark that the maturity and efficiency of the Fourier-domain techniques are leveraged in our problem.

Finally, the performance of the proposed framework will be evaluated in real-life automotive scenarios in terms of resolution, IC, image entropy (IE), and computational complexity (CC).

B. PFA Autofocus

Proposition 1: After the beat signal is compensated with respect to the SRP in (5) using measured radar locations, its phase error due to the localization error is approximated by

$$\epsilon_\phi(n) = k_x(i,n)\hat{\beta}n. \tag{9}$$

Hence, the phase error is compensated by

$$s_C(i,n) \leftarrow \exp\left[-\mathrm{j}k_x(i,n)\hat{\beta}n\right] s_C(i,n) \tag{10}$$

where $\hat{\beta}$ is given by maximizing the IC of the PFA image

$$\hat{\beta} = \arg\max \mathrm{IC}\left(\sigma(x,y)\right). \tag{11}$$

IC is defined as the normalized image variance [24]:

$$\mathrm{IC}\left(\sigma(x,y)\right) \triangleq \frac{\sqrt{\mathrm{mean}\left\{(I-\mathrm{mean}(I))^2\right\}}}{\mathrm{mean}(I)} \tag{12}$$

with $I \triangleq |\sigma(x,y)|^2$ being the image intensity.

Proof: We denote the measured radar location by $[x_r, y_r, z_r]^T$, incorporating a localization error e_x along the track dimension (x). For simplicity, the index n is omitted, though both the location and its error inherently depend on it. The true slant range to a scatterer located at $[x_s, y_s, 0]^T$ is then expressed as

$$r_s^\star \triangleq \sqrt{(x_r + e_x - x_s)^2 + (y_r - y_s)^2 + z_r^2}. \tag{13}$$

Using a Taylor expansion around the measured locations, the slant range can be approximated as follows:

$$r_s^\star \approx r_s + \frac{x_r - x_s}{r_s} e_x \tag{14}$$

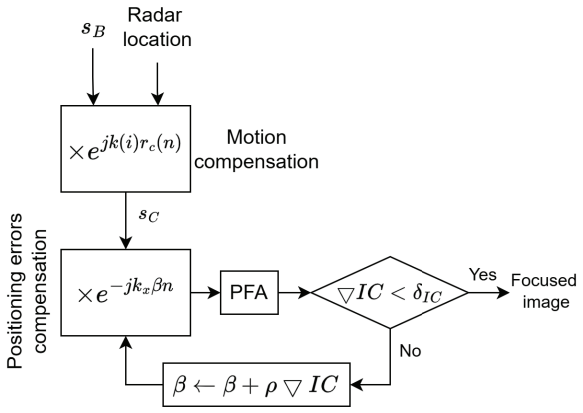

Fig. 2. LECA algorithm. Here, ρ is the learning rate, ∇IC indicates the gradient of the IC, and δ_{IC} is a small value used for stopping the GAA.

where $r_s \triangleq ((x_r - x_s)^2 + (y_r - y_s)^2 + z_r^2)^{1/2}$ is the slant range to the scatterer based on the erroneous measured data. Replacing (14) in (4) gives

$$s_B(i,n) = \sigma(\boldsymbol{s}) \exp\left[-\mathrm{j}k(i) r_s(n)\right] \times \exp\left[-\mathrm{j}k(i) \frac{x_r(n) - x_s}{r_s(n)} e_x(n)\right]. \tag{15}$$

After compensating the measured motion of the radar for the scatterer $\boldsymbol{s}$, we have

$$s_C^\star(i,n) = \sigma(x_s, y_s) \exp\left[-j\left(k_x(i,n)x_s + k_y(i,n)y_s\right)\right] \times \exp\left[-\mathrm{j}k(i) \frac{x_r(n) - x_s}{r_s(n)} e_x(n)\right]. \tag{16}$$

Considering the signals coming from all the scatterers and approximating $(x_r(n) - x_s/r_s(n)) \approx \sin(\alpha_n)$, we get

$$s_C^\star(i,n) = \int_{x_s}\int_{y_s} \sigma(x_s, y_s) \times \exp\left[-j\left(k_x(i,n)x_s + k_y(i,n)y_s\right)\right] \times \exp\left(\mathrm{j}k_x(i,n)e_x\right) \mathrm{d}x_s \mathrm{d}y_s \tag{17}$$

and considering (5), we get

$$s_C^\star(i,n) = \exp\left[\mathrm{j}k_x(i,n)e_x(n)\right] s_C(i,n). \tag{18}$$

This relationship demonstrates that the localization error, $e_x(n)$, manifests itself as a phase error in the compensation of the beat signal with respect to the range to SRP using the *measured* localization data.

To model the error component, we adopt a linear parametric representation, i.e.,

$$e_x(n) = \beta n \tag{19}$$

where β is the parameter representing the linear dependency of the localization error on n. Replacing this model in (18) gives the phase error as given by (9) which can be compensated using (10). ■

Fig. 2 presents the proposed LECA algorithm, using the gradient ascent algorithm (GAA) to rapidly converge to the optimal β value, $\hat{\beta}$.

We now elaborate on three critical observations regarding the localization error model and its implications for SAR image quality.

1) Equation (18) presents the impact of the localization error in only the along-track dimension. It is straightforward to extend the model to include the errors in the other two dimensions as given below

$$s_C^{\star}(i,n) = \exp\left[\mathrm{j}k_x(i,n)\,e_x(n)\right] \times \exp\left[\mathrm{j}k_y(i,n)\,e_y(n)\right] \times \exp\left[\mathrm{j}k(i)\sin(\psi_n)\,e_z(n)\right] s_C(i,n) \quad (20)$$

where $e_y(n)$ and $e_z(n)$, respectively, represent the localization errors in dimensions y and z. Recall that ψ_n denotes the grazing angle of the radar with respect to SRP. The equation above offers more precise error compensation at the expense of increased complexity. However, the vehicle moves primarily along its track dimension x while its movement along the y- and z-axes is minimal during the SAR processing period. As a result, the localization errors, $e_y(n)$ and $e_z(n)$, have a negligible impact and are thus not accounted for in LECA.

2) The linear parametric model (19) considers only the error caused by velocity. Despite its simplicity, this model is sufficient for enhancing SAR image quality because of the following reasons: 1) a zero-degree term is unnecessary since the SRP location is arbitrary, and it is assumed to be zero at $n = 0$ and 2) while higher degree terms could potentially improve the image focus, they introduce additional complexity, which is not desirable in SAR processing.

3) Equation (18) shows that the localization error manifests in the cross-range dimension. Rewriting (17) gives

$$s_C^{\star}(i,n) = \int_{x_s}\int_{y_s} \sigma(x_s,y_s) \times \exp\left\{-j\left[k_x(i,n)\left(x_s + e_x(n)\right) + k_y(i,n)\,y_s\right]\right\} \mathrm{d}x_s\mathrm{d}y_s. \quad (21)$$

This indicates that the error primarily affects the area around the SRP in the cross-range dimension. In other words, we should focus on image improvements in the vicinity of the SRP, as the error has minimal impact on more distant areas. Naturally, the PFA algorithm performs well mainly in areas close to the SRP, while distortion increases farther away.

C. BPA Autofocus

BPA relies on precise radar location for each chirp, as shown in (8). Localization errors result in inaccurate range interpolation across all the image pixels, leading to significant image distortion. Implementing autofocus algorithms by optimizing an image quality metric over radar locations is computationally intensive, as it necessitates correcting the range for each individual image pixel, significantly increasing the complexity of the BPA process. To address this challenge, the localization error estimated using PFA is leveraged. Accordingly, we propose two approaches to enhance the focus of BPA.

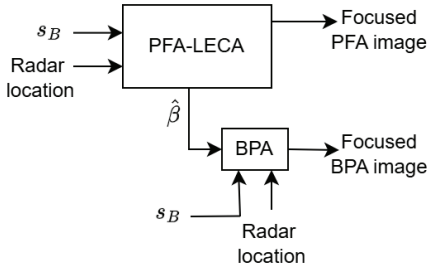

Fig. 3. LECA-IC for BPA autofocus. The localization error parameter is estimated by maximizing IC by PFA-LECA.

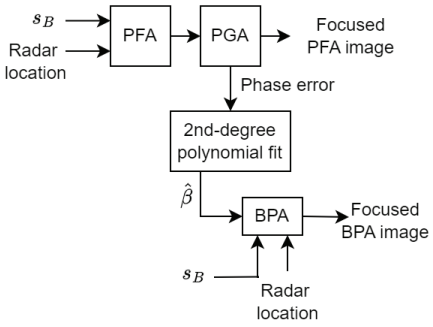

Fig. 4. LECA with PGA for BPA autofocus.

1) LECA With IC Maximization: Once the localization error $e_x(n)$ is obtained by maximizing IC using PFA-LECA, it can be used to correct the localization data of backprojection. Specifically, before backprojection (8), x_r should be corrected by $x_r(n) \leftarrow x_r(n) + \hat{\beta}n$. Fig. 3 illustrates the pipeline of this method referred to as LECA-IC.

2) LECA With PGA: PGA [25] provides a computationally efficient solution to estimate the phase error. It assumes that each range bin of the SAR image is dominated by at most one major scatterer and proves that the phase error spectrum is modulated by that major scatterer. Then, it estimates the phase error gradient by exploiting the redundancy across the major scatterers of the image. Consequently, the phase error is calculated by accumulation of the phase gradient. Since PGA incorporates no intense optimization, it is fast and has been adopted extensively in practical SAR systems. Furthermore, the high SNR resulting from the presence of strong scatterers makes automotive applications particularly well-suited for this autofocus algorithm.

While PGA estimates the phase error, (18) gives an insight on how it can be related to the localization error. More specifically, using (19) in (18) gives the phase error as

$$k_x(i,n)\,e_x(n) = k(i)\,\alpha'\beta n^2 \quad (22)$$

wherein the approximation $\sin(\alpha_n) \approx \alpha' n$ is used. Since the quadratic phase error is dominant in SAR imaging [26], the phase error given by PGA, $\epsilon_\phi(n)$, can be approximated by a second-degree polynomial, i.e., $\epsilon_\phi \approx q_0 + q_1 n + q_2 n^2$. Then, an approximation of β is given by

$$\hat{\beta} = \frac{q_2}{\bar{k}_i \alpha'} \quad (23)$$

TABLE I
SETTING OF THE RADAR USED IN THE AUTOMOTIVE SCENARIO OF THE DEEPSENSE 6G DATASET

f_c (GHz)	B (MHz)	PRT[1](T_c) (μs)	CPI (ms)	N_c	S^2	F_s[3] (MHz)
77.45	900.9	65	100	128	256	5

[1] Pulse repetition time.
[2] Number of samples per chirp.
[3] Receiver sampling frequency.

where $\bar{k}_i$ denotes the average of $k(i)$ over the fast time index i. The pipeline of using PGA for the BPA autofocus, referred to as LECA-PGA, is depicted in Fig. 4.

Here, we highlight two points to note.

1) In our proposed PFA-based autofocus method for BPA, alternative variants of BPA—such as FBP [27], [28], FFBP [29], and multistage BP [30]—can also be used to enhance imaging efficiency by reducing overall computational complexity.
2) PFA is a spotlight SAR algorithm assisting BPA, a stripmap SAR algorithm, in autofocus. Spotlight algorithms require a designated SRP from which the imaging process is referenced. This requirement, however, does not impose significant constraints, provided that the operational limitations of PFA and PGA algorithm are respected. For PFA, SRP must be positioned at a sufficient distance from the sensor such that the linear trajectory of the platform approximates a circular arc over the synthetic aperture. This far-field condition minimizes wavefront curvature errors and ensures accurate image formation. In addition, excessive squint angles introduce range-dependent phase errors, compromising the planar wavefront assumption central to PFA and degrading image quality. Regarding PGA, large SAR CPIs must be avoided to prevent degradation of SNR due to temporal coherence loss or motion-induced decorrelation. PGA relies on robust SNR to accurately estimate phase gradients and correct residual phase errors across the aperture. If the CPI is excessively prolonged, coherence between pulses may diminish due to environmental changes or uncompensated motion, reducing SNR and impairing PGA ability to refine image focus.

IV. EXPERIMENTAL RESULTS

In what follows, we present the experimental results of the proposed autofocus algorithms in an automotive scenario.

A. Experimental Scenario and Methods

We evaluate the proposed autofocus algorithms in the automotive scenario of the DeepSense 6G dataset [31]. Specifically, we use the data of the radar looking at the right side of the car when it moves along a rural road. The car velocity along its track is about 17.5 m/s with negligible motion along the other directions. The radar used is an MIMO FMCW radar with the parameters shown in Table I. The radar has one transmitter and four receivers creating four virtual receive antennas aligned along the car track.

The dataset includes vehicle locations recorded by a high-precision GPS at a rate of ten updates/s. These GPS locations are interpolated at each chirp instant. However, since the interpolated locations are not entirely accurate, an autofocus algorithm is necessary to correct the resulting phase errors.

Since the radar is MIMO with four channels, the impact of the autofocus algorithms is evaluated in the following SAR processing pipelines.

1) PFA after beamforming with respect to the SRP. During the evaluations, we place the SRP of PFA at 22 m on the right side of the car.
2) SISO BPA where only one channel is used for backprojection.
3) Pre-BPA BF wherein beamforming is performed with respect to the radar boresight by coherently averaging the data of the virtual receive antennas. With this, the radar beam is narrowed down before running BPA.
4) BPA with pixelwise BF where beamforming is performed per pixel before backprojection.

Regarding the performance-complexity tradeoff in the above pipelines, we anticipate the following points.

1) The PFA images get distorted in the areas distant from the SRP. Furthermore, both the PGA and LECA improve the PFA focus only in the vicinity of the SRP while negligible improvements can be expected in other areas, as discussed in Section III-B.
2) Beamforming improves the image SNR, translating into larger IC and smaller IE values.
3) BPA with pixelwise BF gives the best imaging quality at the expense of higher complexity.

The above four SAR processing pipelines are quantitatively compared in terms of the following metrics.

1) *Azimuth Resolution (AR):* Defined as the distance between the points with 3 dB below the maximum power of the main lobe peak in the azimuth direction [32], [33]. We report the AR averaged across the five strongest scatterers.
2) *IC:* As defined in (12).
3) *Image Entropy (IE):* Given by $\text{IE} \triangleq -\sum_{i=1}^{L} p_i \log_2(p_i)$ where image intensities are divided into L levels, and p_i represents the probability of intensities falling within the ith level. We use $L = 256$.
4) *Computational Complexity (CC):* Measured as the runtime of each algorithm on a laptop equipped with an Intel 11th Gen Core i7-1185G7 CPU and 32-GB RAM.

B. Results and Discussion

Three instances of SAR results using the above-mentioned processing pipelines are shown in Figs. 5–7 along with their quantified comparison listed in Table II.

Fig. 5 illustrates the imaging result when crossing a railway. As shown in 5(b), both the autofocus algorithms have narrowed the width of the main lobes in PFA. As expected, the PFA images get distorted in areas distant from SRP while this is not the case with BPA. In all the BPA processing pipelines, both the autofocus algorithms have improved the image focus. Beamforming, particularly pixelwise BF, further

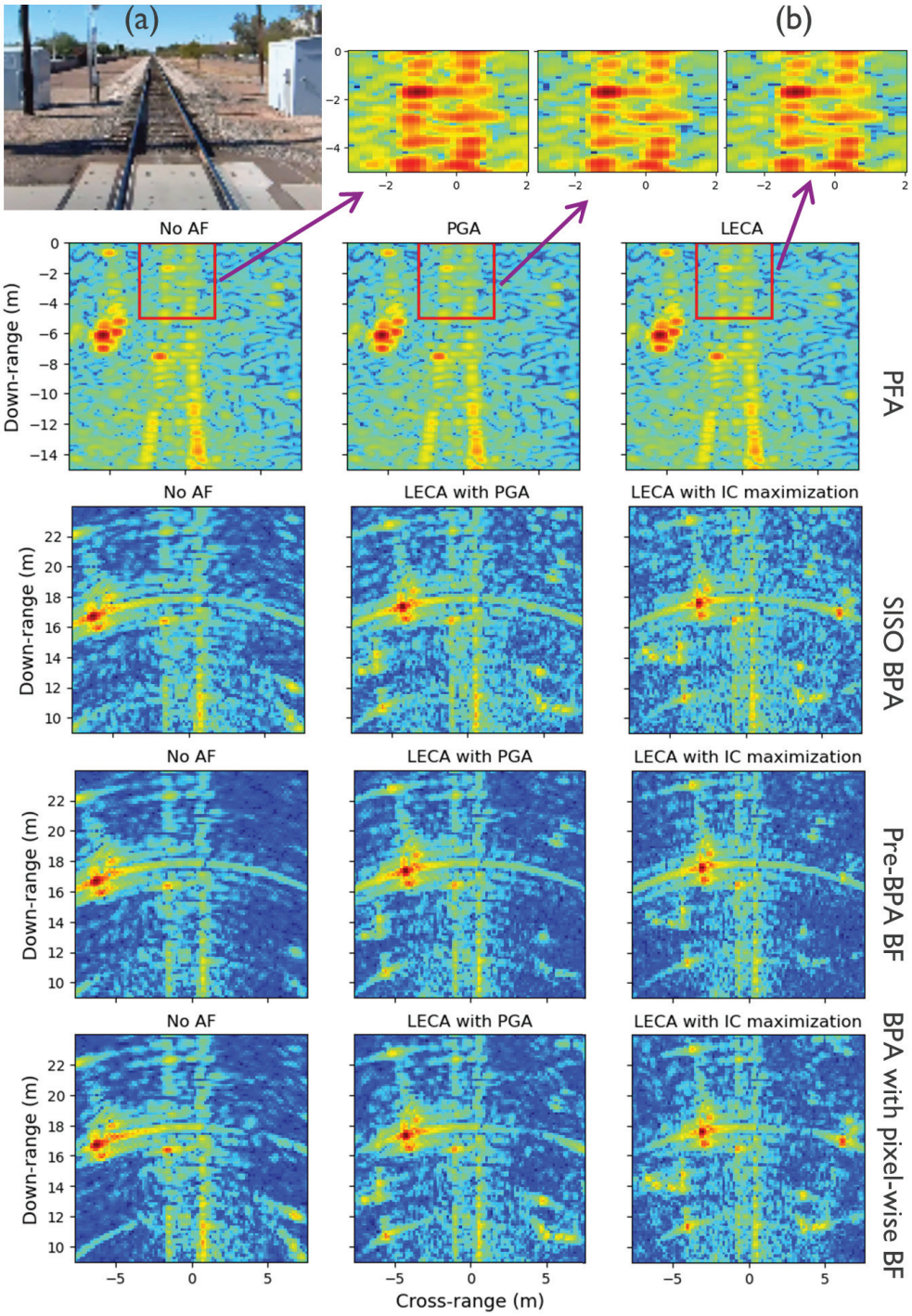

Fig. 5. Example #1. (a) Camera image of the SAR target scene. (b) Zoomed-in areas of specified in the PFA SAR images. The other rows depict the results of different scenarios of SAR imaging.

improves imaging quality in BPA by better preserving scatterers and reducing sidelobes compared with pre-BPA BF. However, this improvement comes at the cost of significantly increased complexity.

In Fig. 6, the target scene consists of a building, a tree with foliage, a short wall, and various other details such as light poles. In the reconstructed SAR images, the building area is highlighted by a red rectangle. As seen, the foliage and the wall have been clearly pictured by PFA but the building is not well-detected. In the BPA processing pipelines, the impact of autofocus is evident in the detection of the building and the light poles. Here, the building details are faded by pre-BPA BF, whereas BPA with pixelwise BF reconstructs them well.

The last example in Fig. 7 demonstrates the advantage of BPA with pixelwise BF over other methods in reconstructing scene details, including the roadsides, foliage, and light poles. The impact of autofocus algorithms is evident in the improved azimuth resolution. In addition, the parked car is detected in

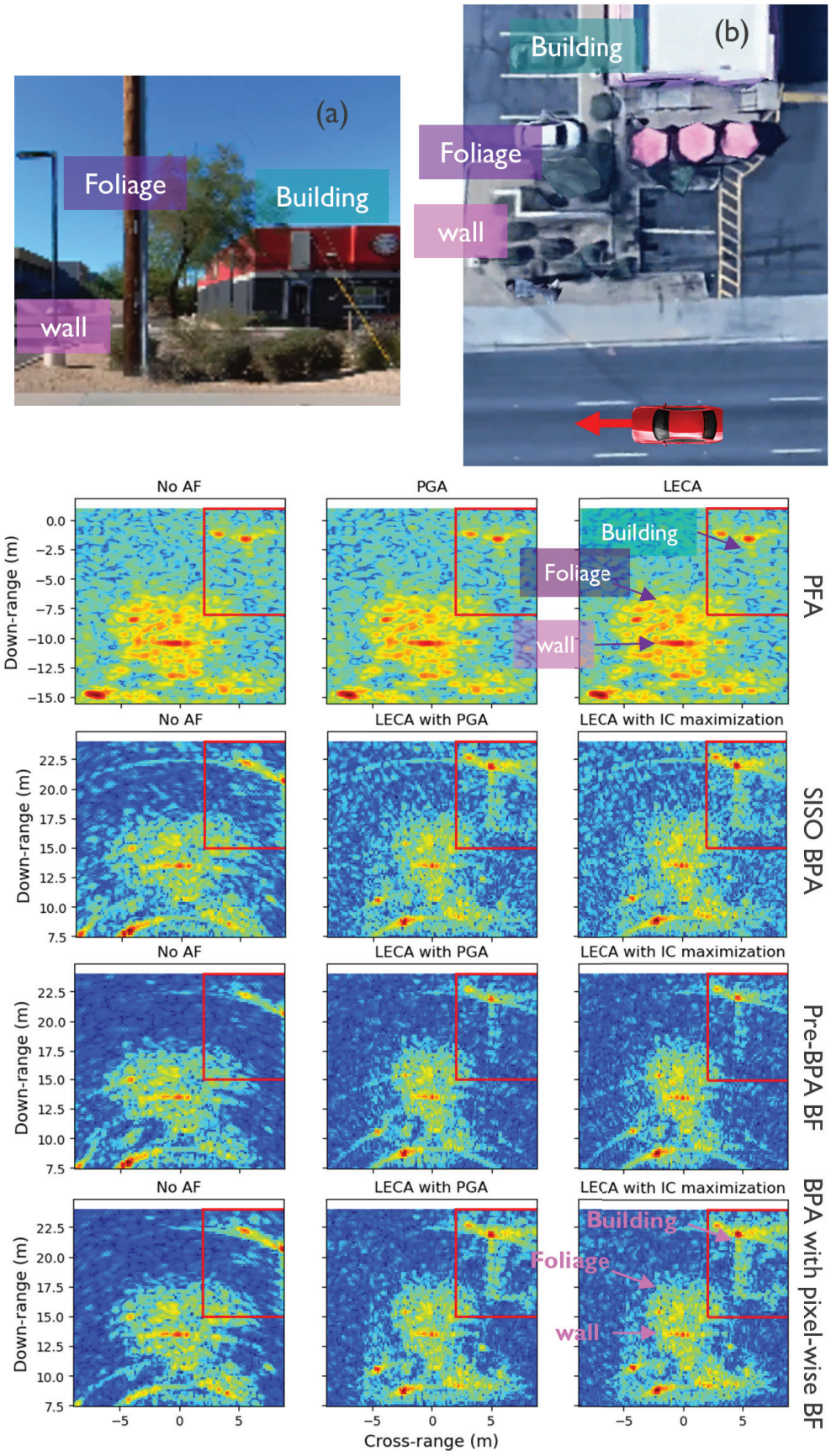

Fig. 6. Example #2. (a) Camera image of the target scene of SAR imaging. (b) Bird's eye view of the target scene from Google Maps [34] with the red arrow indicating the car trajectory. The other rows depict the results of different processing pipelines of SAR imaging with the building area highlighted by red rectangles.

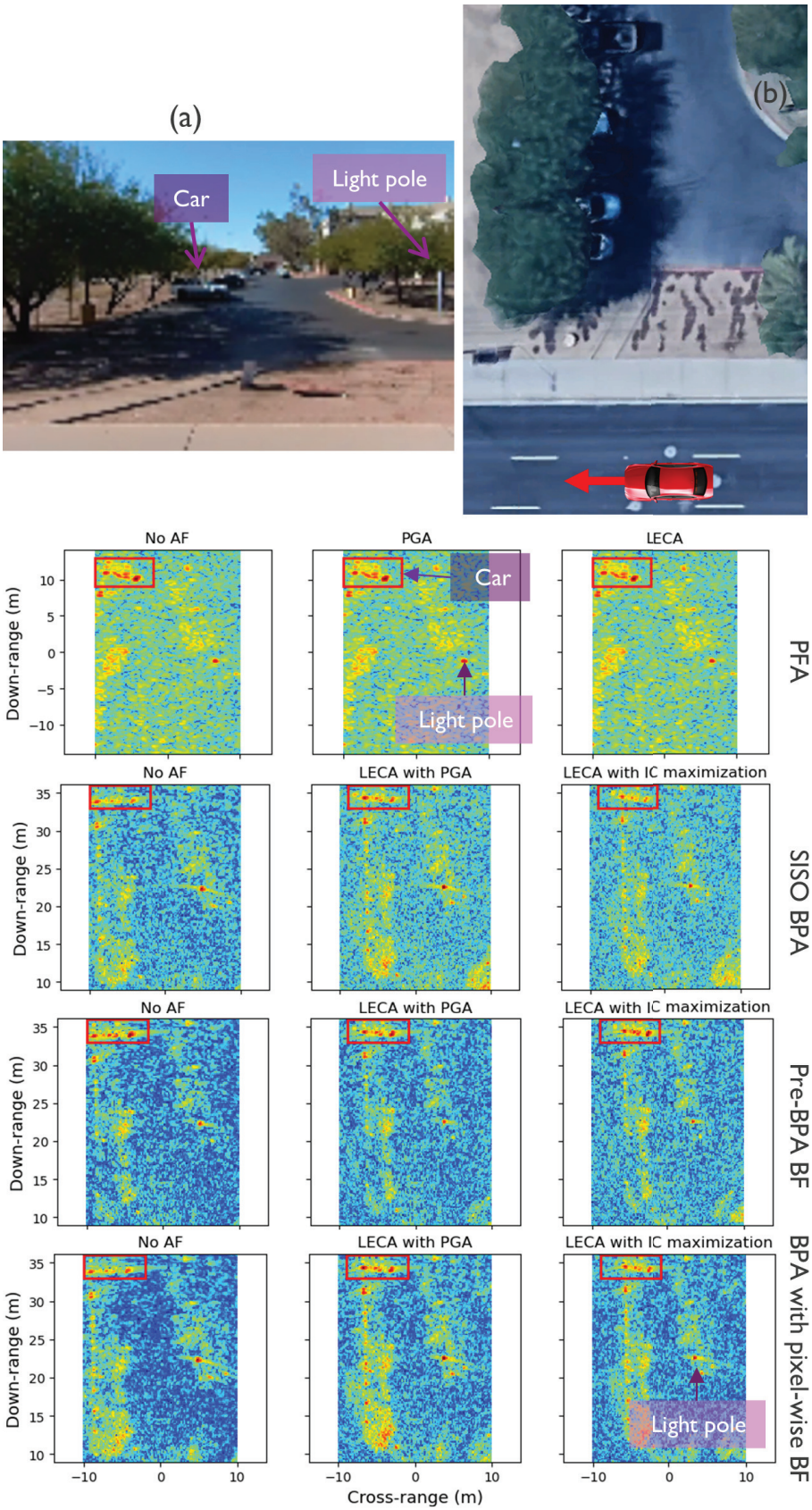

Fig. 7. Example #3. (a) Camera image of the target scene of SAR imaging. (b) Bird's eye view of the target scene from Google Maps [34] with the red arrow indicating the car trajectory. The other rows depict the results of different processing pipelines of SAR imaging, with the car area highlighted by red rectangles.

TABLE II
COMPARISON OF DIFFERENT SCENARIOS OF SAR IMAGING IN THE EXAMPLES SHOWN IN FIGS. 5–7. THE BEST VALUES IN EACH IMAGING PROCESSING PIPELINE ARE HIGHLIGHTED WHILE THE BEST VALUES AMONG THE BPA PROCESSING PIPELINES ARE UNDERLINED

Ex.	Metric	PFA			SISO BPA			Pre-BPA BF			BPA with pixel-wise BF		
		No AF[1]	PGA	LECA	No AF	LP[2]	LI[3]	No AF	LP	LI	No AF	LP	LI
#1	AR[4]	**0.77**	0.77	0.77	0.89	0.55	**0.47**	0.85	0.68	**0.72**	0.81	0.64	**0.47**
	IC[5]	60.13	**60.46**	60.23	29.28	32.82	**37.07**	30.50	36.62	**41.97**	20.62	30.13	**35.90**
	IE[6]	0.52	**0.51**	0.51	1.94	1.86	**1.57**	1.53	1.37	**1.09**	2.43	1.68	**1.26**
	CC[7]	**0.27**	0.27	58.38	**0.19**	0.46	58.57	**0.19**	0.46	58.57	**232.23**	242.06	288.90
#2	AR	2.04	**1.85**	1.97	0.81	0.60	**0.51**	0.81	0.60	**0.51**	0.85	0.60	**0.51**
	IC	28.71	**29.68**	28.93	16.01	20.32	**21.58**	19.06	25.36	**26.34**	13.86	19.96	**21.79**
	IE	1.15	**1.10**	1.14	2.65	**2.26**	2.43	2.24	**1.75**	1.93	2.63	**2.04**	2.17
	CC	**0.17**	0.27	37.91	**0.19**	0.44	38.08	**0.22**	0.45	38.10	**218.34**	222.30	256.28
#3	AR	**1.32**	1.32	1.32	0.60	**0.55**	0.55	0.68	0.72	**0.55**	0.60	**0.55**	0.60
	IC	24.91	25.07	**25.09**	9.55	7.54	**9.57**	9.43	9.46	**10.04**	9.42	**8.01**	9.75
	IE	2.30	**2.29**	2.29	3.58	4.06	**3.50**	3.96	**3.74**	3.80	3.44	3.94	**3.40**
	CC	**0.76**	0.77	131.10	**0.19**	0.96	131.31	**0.20**	0.96	131.29	**222.20**	222.77	350.46

[1] Autofocus
[2] Localization error compensation by PGA
[3] Localization error compensation by IC maximization
[4] Azimuth resolution (m)
[5] Image contrast
[6] Image entropy
[7] Computational complexity (s)

all the SAR processing pipelines, although it appears blurred without autofocus.

The quantitative comparison in Table II highlights the significant improvement in azimuth resolution achieved by BPA. It is evident that the resolution is consistently enhanced by either autofocus algorithm. However, IC maximization entails much higher complexity. Furthermore, while the pre-BPA BF is shown to achieve the best performances in most cases, it is important to note that some image details may be missed due to beamforming with respect to the radar boresight, as particularly observed in example #2.

C. Computational Complexity of the SAR Processing Pipelines and Autofocus Algorithms

The following assumes that the image size is $N \times N$ reconstructed based on N_c pulses where each pulse contains N_s samples.

1) PFA: The total complexity of PFA is dominated by 2D-FFT with a complexity of $\mathcal{O}(N^2 \log N)$.

2) SISO BPA: In SISO BPA, each image pixel is reconstructed by backprojecting the range-compressed pulses resulting in a complexity of $\mathcal{O}(N_c N^2)$.

3) PGA: The PGA steps, respectively, consist of IFT, center shifting, FFT, and a maximum likelihood estimation. These operations are executed for J major scatterers within the image for a few iterations (typically fewer than 10). Consequently, the complexity of each PGA iteration is primarily influenced by IFT and FFT, resulting in an overall complexity of $\mathcal{O}(JN \log N)$.

4) LECA: The LECA algorithm, as illustrated in Fig. 2, performs GAA to maximize the PFA IC. If the optimization takes T iterations, the total complexity will be $\mathcal{O}(TN^2 \log N)$.

5) Pre-BPA BF: For a linear array including N_v virtual antennas, beamforming with respect to, the radar boresight is equivalent to summing the received chirps at N_v receive antennas. The complexity of beamforming is added to that of BPA giving a complexity of $\mathcal{O}(N_v N_c N_s + N_c N^2)$.

6) BPA With Pixelwise BF: Since beamforming is conducted on a per-pixel basis, the complexity of this SAR processing pipeline is $\mathcal{O}(N_v N_c N_s N^2)$. This makes BPA with pixelwise BF the most complex SAR processing pipeline.

As shown in the evaluation results, PGA has a negligible computational burden, whereas LECA's complexity may increase depending on its convergence rate. Meanwhile, pre-BPA BF with PGA-based localization error compensation provides a reasonable tradeoff between complexity and quality, as confirmed by Table II. However, BPA with pixelwise BF, though significantly more complex than other pipelines, excels at sidelobe suppression and detail enhancement, as evident in Figs. 5–7. Notably, the above complexity analysis assumes sequential processing, whereas parallel processing on an FPGA [35] or GPU [36], [37] can significantly reduce computational demands.

V. CONCLUSION

In this article, we studied the impact of the localization error on SAR imaging with automotive FMCW radars. To this end, we began with the PFA. We identified that localization error manifests itself as a phase error in the beat signal after compensation with respect to the range to the SRP.

We introduced the LECA technique, which determines the localization error parameter by optimizing the IC. Building on this, we proposed the LECA-IC algorithm for the BPA, where localization errors are corrected using IC maximization derived from PFA to enhance image focusing. Furthermore,

we developed the LECA-PGA algorithm for BPA, leveraging the simplicity and effectiveness of PGA for localization error estimation. Due to PGA's low complexity, this approach provides an extremely efficient autofocus solution for BPA.

Ultimately, we showed our algorithms' effectiveness in an automotive scenario. While we showed the effectiveness of the proposed autofocus algorithms in side-looking SAR (SL-SAR), they are applicable in other SAR configurations, including forward-looking SAR (FL-SAR) [38], [39] where the localization errors have a similar impact. By addressing the challenges of localization errors in SAR imaging for automotive applications, this study sets a foundation for further advancements in efficient and accurate SAR imaging techniques, ensuring robust performance under real-world conditions.

ACKNOWLEDGMENT

The authors thank Dr. Eddy De Greef for his support in the experimental evaluations conducted in the laboratory.

REFERENCES

[1] S. Yao et al., "Radar-camera fusion for object detection and semantic segmentation in autonomous driving: A comprehensive review," *IEEE Trans. Intell. Vehicles*, vol. 9, no. 1, pp. 2094–2128, Jan. 2024.

[2] A. Venon, Y. Dupuis, P. Vasseur, and P. Merriaux, "Millimeter wave FMCW RADARs for perception, recognition and localization in automotive applications: A survey," *IEEE Trans. Intell. Vehicles*, vol. 7, no. 3, pp. 533–555, Sep. 2022.

[3] S. Gishkori, L. Daniel, M. Gashinova, and B. Mulgrew, "Imaging for a forward scanning automotive synthetic aperture radar," *IEEE Trans. Aerosp. Electron. Syst.*, vol. 55, no. 3, pp. 1420–1434, Jun. 2019.

[4] G. Franceschetti and R. Lanari, *Synthetic Aperture Radar Processing*. Boca Raton, FL, USA: CRC Press, 1999.

[5] M. A. Richards, *Fundamentals of Radar Signal Processing*, 2nd ed., New York, NY, USA: McGraw-Hill, 2014.

[6] J. A. M. Armin, W. Doerry, and E. E. Bishop, "Basics of backprojection algorithm for processing synthetic aperture radar images," Sandia National Laboratories, Albuquerque, NM, USA, Tech. Rep. SAND2012-3369, Feb. 2016.

[7] A. W. Doerry, "Basics of polar-format algorithm for processing synthetic aperture radar images," Sandia National Laboratories, Albuquerque, NM, USA, Tech. Rep. SAND2012-3369, May 2012.

[8] M. Heidbrink, O. Sura, V. K. Rangaraj, M. Reinecke, M. Hoffmann, and M. Vossiek, "Concept for automatic annotation of automotive radar data using AI-segmented camera and LiDAR reference data," in *Proc. 21st Eur. Radar Conf. (EuRAD)*, Sep. 2024, pp. 292–295.

[9] S. Tebaldini et al., "Sensing the urban environment by automotive SAR imaging: Potentials and challenges," *Remote Sens.*, vol. 14, no. 15, p. 3602, Jul. 2022.

[10] H. Iqbal, A. Löffler, M. N. Mejdoub, D. Zimmermann, and F. Gruson, "Imaging radar for automated driving functions," *Int. J. Microw. Wireless Technol.*, vol. 13, no. 7, pp. 682–690, Sep. 2021.

[11] X. Gao, S. Roy, and G. Xing, "MIMO-SAR: A hierarchical high-resolution imaging algorithm for mmWave FMCW radar in autonomous driving," *IEEE Trans. Veh. Technol.*, vol. 70, no. 8, pp. 7322–7334, Aug. 2021.

[12] B. Zhang, G. Xu, R. Zhou, H. Zhang, and W. Hong, "Multi-channel back-projection algorithm for mmWave automotive MIMO SAR imaging with Doppler-division multiplexing," *IEEE J. Sel. Topics Signal Process.*, vol. 17, no. 2, pp. 445–457, Mar. 2023.

[13] M. G. Polisano, M. Manzoni, S. Tebaldini, A. Monti-Guarnieri, C. M. Prati, and I. Russo, "Very high resolution automotive SAR imaging from burst data," *Remote Sens.*, vol. 15, no. 3, p. 845, Feb. 2023.

[14] M. G. Polisano, M. Manzoni, S. Tebaldin, A. V. Monti-Guarnieri, C. M. Prati, and I. Russo, "Automotive MIMO-SAR imaging from non-continuous radar acquisitions," in *Proc. Photon. Electromagn. Res. Symp. (PIERS)*, Jul. 2023, pp. 578–587.

[15] D. Tagliaferri et al., "Navigation-aided automotive SAR for high-resolution imaging of driving environments," *IEEE Access*, vol. 9, pp. 35599–35615, 2021.

[16] H. Iqbal, M. B. Sajjad, M. Mueller, and C. Waldschmidt, "SAR imaging in an automotive scenario," in *Proc. IEEE 15th Medit. Microw. Symp. (MMS)*, Nov. 2015, pp. 1–4.

[17] G. Ciaramitaro et al., "On the minimum set of navigation sensors to enable high-resolution automotive SAR imaging," in *Proc. IEEE Radar Conf. (RadarConf)*, May 2023, pp. 1–6.

[18] R. K. Raney, H. Runge, R. Bamler, I. G. Cumming, and F. H. Wong, "Precision SAR processing using chirp scaling," *IEEE Trans. Geosci. Remote Sens.*, vol. 32, no. 4, pp. 786–799, Jul. 1994.

[19] I. J. Gupta and S. Haykin, "A comparison of various deconvolution algorithms for synthetic aperture radar imagery," *IEEE Trans. Antennas Propag.*, vol. AP-29, no. 4, pp. 632–638, 1981.

[20] D. E. Wahl, P. H. Eichel, D. C. Ghiglia, and C. V. Jakowatz, "Phase gradient autofocus—A robust tool for high resolution SAR phase correction," *IEEE Trans. Aerosp. Electron. Syst.*, vol. 30, no. 3, pp. 827–835, Jul. 1994.

[21] C. V. JakowatzJr., D. E. Wahl, and P. H. Eichel, D. C. Ghiglia, and P. A. Thompson, *Spotlight-Mode Synthetic Aperture Radar: A Signal Processing Approach*. Norwell, MA, USA: Kluwer, 1996.

[22] T. Xiong, M. Xing, Y. Wang, S. Wang, J. Sheng, and L. Guo, "Minimum-entropy-based autofocus algorithm for SAR data using Chebyshev approximation and method of series reversion, and its implementation in a data processor," *IEEE Trans. Geosci. Remote Sens.*, vol. 52, no. 3, pp. 1719–1728, Mar. 2014.

[23] R. L. Morrison, M. N. Do, and D. C. Munson, "SAR image autofocus by sharpness optimization: A theoretical study," *IEEE Trans. Image Process.*, vol. 16, no. 9, pp. 2309–2321, Sep. 2007.

[24] M. Martorella, F. Berizzi, and B. Haywood, "Contrast maximisation based technique for 2-D ISAR autofocusing," *IEE Proc.-Radar, Sonar Navigat.*, vol. 152, no. 4, pp. 253–262, 2005.

[25] D. E. Wahl, F. H. Eichel, D. C. Ghiglia, and C. V. Jakowatz, "Phase gradient autofocus-a robust tool for high resolution SAR phase correction," *IEEE Trans. Aerosp. Electron. Syst.*, vol. 30, no. 3, pp. 827–835, Jul. 1994.

[26] D. C. Ghiglia and M. D. Pritt, *Two-Dimensional Phase Unwrapping: Theory, Algorithms, and Software*. New York, NY, USA: Wiley, 1998.

[27] A. F. Yegulalp, "Fast backprojection algorithm for synthetic aperture radar," in *Proc. IEEE Radar Conf. Radar Into Next Millennium*, Apr. 1999, pp. 60–65.

[28] J. W. McCorkle and M. Rofheart, "Order N^2 log(N) backprojector algorithm for focusing wide-angle wide-bandwidth arbitrary-motion synthetic aperture radar," *Proc. SPIE*, vol. 2747, pp. 25–36, Jun. 1996, doi: 10.1117/12.243085.

[29] L. M. H. Ulander, H. Hellsten, and G. Stenstrom, "Synthetic-aperture radar processing using fast factorized back-projection," *IEEE Trans. Aerosp. Electron. Syst.*, vol. 39, no. 3, pp. 760–776, Jul. 2003.

[30] Q. Zheng, S. Shang, Y. Li, and Y. Zhu, "A novel multistage back projection fast imaging algorithm for terahertz video synthetic aperture radar," *Remote Sens.*, vol. 15, no. 10, p. 2602, May 2023.

[31] A. Alkhateeb et al., "DeepSense 6G: A large-scale real-world multi-modal sensing and communication dataset," *IEEE Commun. Mag.*, vol. 61, no. 9, pp. 122–128, Sep. 2023.

[32] A. Martinez and J. L. Marchand, "SAR image quality assessment," *Revista de Telección*, vol. 2, pp. 1–7, Jan. 1993.

[33] H. Zhang, Y. Li, and Y. Su, "SAR image quality assessment using coherent correlation function," in *Proc. 5th Int. Congr. Image Signal Process.*, Oct. 2012, pp. 1129–1133.

[34] Google.*Google Maps*. Accessed: Oct. 12, 2024. [Online]. Available: https://www.google.com/maps

[35] D. Mota et al., "Onboard processing of synthetic aperture radar back-projection algorithm in FPGA," *IEEE J. Sel. Topics Appl. Earth Observ. Remote Sens.*, vol. 15, pp. 3600–3611, 2022.

[36] A. Capozzoli, C. Curcio, and A. Liseno, "Fast GPU-based interpolation for SAR back-projection," *Prog. Electromagn. Res.*, vol. 133, pp. 259–283, 2013.

[37] P. Lasserre. (2009). *Unlocking the Benefits of SAR Back Projection*. Accessed: Feb. 18, 2025. [Online]. Available: https://gsitechnology.com/unlocking-the-benefits-of-sar-back-projection/

[38] A. Albaba, A. Sakhnini, H. Sahli, and A. Bourdoux, "Forward-looking MIMO-SAR for enhanced angular resolution," in *Proc. IEEE Radar Conf. (RadarConf)*, New York City, NY, USA, Mar. 2022, pp. 1–6.

[39] A. Albaba, M. Bauduin, T. Verbelen, H. Sahli, and A. Bourdoux, "Forward-looking MIMO-SAR for enhanced radar imaging in autonomous mobile robots," *IEEE Access*, vol. 11, pp. 66934–66948, 2023.

S. Hamed Javadi (Member, IEEE) received the B.S. degree in electrical engineering from the Ferdowsi University of Mashhad, Mashhad, Iran, in 2005, the M.S. degree from the Department of Electronic, K. N. Toosi University of Technology, Tehran, Iran, in 2008, and the Ph.D. degree from the Ferdowsi University of Mashhad, in 2013.

From 2013 to 2019, he was an Assistant Professor with the University of Bojnord, Bojnord, Iran, where he focused on statistical signal processing, distributed algorithms, and machine learning and was involved in several international projects. Following his academic role, he worked as a Postdoctoral Researcher with the Department of Environment, Ghent University, Ghent, Belgium, where he developed efficient AI-based algorithms for smart farming using data from multiple sensors. Currently, he is a Researcher with IMEC, Leuven, Belgium, where he specializes in signal processing, radar imaging, sensor fusion, and AI.

André Bourdoux (Senior Member, IEEE) received the M.Sc. degree in electrical engineering from the Universite Catholique de Louvain, Ottignies-Louvain-la-Neuve, Belgium, in 1982.

He joined the Interuniversity Microelectronics Center (IMEC), Leuven, Belgium, in 1998, where he is the Scientific Director with the Advanced RF Research Group. He is a system-level and signal processing expert for both the mmwave wireless communications and radar teams. He has more than 15 years of research experience in radar systems and broadband wireless communications. He holds several patents in these fields. He has authored or co-authored over 180 publications in books and peer-reviewed journals and conferences. His research interests include advanced architectures, signal processing and machine learning for wireless physical layers, and high-resolution 3-D/4-D radars.

Adnan Albaba received the B.Sc. degree in biomedical engineering from Jordan University of Science and Technology (JUST), Irbid, Jordan, in 2016, and the M.Sc. degree in embedded systems from Uppsala Universitet (UU), Uppsala, Sweden, in 2019. He is currently pursuing the Ph.D. degree in engineering sciences with Vrije Universiteit Brussel (VUB), Brussels, Belgium, in collaboration with the Interuniversity Microelectronics Centre (IMEC), Leuven, Belgium.

His main research interests include radar systems and signal processing, radar imaging, synthetic aperture radar, and biomedical systems and signal processing.

Hichem Sahli is currently a Professor in computer vision and machine learning with the Department of Electronics and Informatics, Vrije Universiteit Brussel (VUB), Brussels, Belgium, and the Principal Scientist with Interuniversitair Micro-Elektronica Centrum (IMEC) VZW, Leuven, Belgium. He has completed 28 Ph.D. Supervisions since 2000, when he joined IMEC and VUB. He has co-authored over 300 journal articles, conference publications, and book chapters. His research focuses on signal processing, computer vision, and machine learning theory and algorithms in AI for computer vision (image, radar, and video processing), affective computing, health informatics (disease progression prediction, diagnosis, and treatment outcome prediction), and natural language processing (electronic health record coding).